coatings

MDPI

Article

Crystalline Structure and Optical Properties of Cobalt Nickel Oxide Thin Films Deposited with a Pulsed Hollow-Cathode Discharge in an Ar+O_2 Gas Mixture

Anna Kapran [1,2], Rainer Hippler [1,3,*], Harm Wulff [3], Jiri Olejnicek [1], Lenka Volfova [1], Aneta Pisarikova [1,4], Natalia Nepomniashchaia [1,5], Martin Cada [1] and Zdenek Hubicka [1]

1 Institute of Physics, Czech Academy of Sciences, Na Slovance 2, 18221 Prague, Czech Republic; kapran@fzu.cz (A.K.); olejn@fzu.cz (J.O.); volfl@fzu.cz (L.V.); hrubantova@fzu.cz (A.P.); nepomni@fzu.cz (N.N.); cada@fzu.cz (M.C.); hubicka@fzu.cz (Z.H.)
2 Faculty of Mathematics and Physics, Charles University, Ke Karlovu 3, 12116 Prague, Czech Republic
3 Institut für Physik, Universität Greifswald, Felix-Hausdorff-Str. 6, 17489 Greifswald, Germany; wulff@uni-greifswald.de
4 Joint Laboratory of Optics, Palacky University Olomouc, Av. 17. listopadu 50A, 77207 Olomouc, Czech Republic
5 Faculty of Nuclear Sciences and Physical Engineering, Czech Technical University in Prague, Brehova 7, 11519 Prague, Czech Republic
* Correspondence: hippler@physik.uni-greifswald.de

Abstract: Cobalt nickel oxide films are deposited on Si(111) or fluorine-doped tin-oxide-coated (FTO) glass substrates employing a pulsed hollow-cathode discharge. The hollow cathode is operated with argon gas flowing through the nozzle and with O_2 gas admitted to the vacuum chamber. Three different cathode compositions (Co20Ni80, Co50Ni50, and Co80Ni20) are investigated. Deposited and annealed thin films are characterized by X-ray diffraction, infrared (Raman) spectroscopy, and ellipsometry. As-deposited films consist of a single mixed cobalt nickel oxide phase. Upon annealing at 600 °C, the mixed cobalt nickel oxide phase separates into two cystalline sub-phases which consist of cubic NiO and cubic Co_3O_4. Annealed films are investigated by spectroscopic ellipsometry and the optical bandgaps are determined.

Keywords: hollow-cathode discharge; mixed cobalt nickel oxide film; refractive index; absorption coefficient; optical bandgap

Citation: Kapran, A.; Hippler, R.; Wulff, H.; Olejnicek, J.; Volfova, L.; Pisarikova, A.; Nepomniashchaia, N.; Cada, M.; Hubicka, Z. Crystalline Structure and Optical Properties of Cobalt Nickel Oxide Thin Films Deposited with a Pulsed Hollow-Cathode Discharge in an Ar+O_2 Gas Mixture. *Coatings* **2024**, *14*, 319. https://doi.org/10.3390/coatings14030319

Academic Editors: Tsvetanka Babeva, Gergana Alexieva and Rositsa Gergova

Received: 29 January 2024
Revised: 26 February 2024
Accepted: 1 March 2024
Published: 6 March 2024

1. Introduction

Mixed metal oxides (MMO) consist of two or more metal atoms in combination with oxygen. Mixed cobalt nickel oxides (CoNiO) have received renewed interest in the past years [1]. Non-stoichiometric CoNiO and stoichiometric $NiCo_2O_4$ are of interest for many applications, e.g., as batteries [2–6], supercapacitors [7,8], battery supercapacitor hybrids [9], sensors [10], solar cells [11], and catalysts [12–16]. Here, we are guided by an interest in the crystallographic and optical properties of deposited CoNiO films with varying Co/Ni ratios. Both cobalt oxide and nickel oxide are p-type semiconductors. The optical bandgaps of cobalt oxide and nickel oxide are rather different. NiO has a direct optical bandgap of about 3.8–4.1 eV [17–20]. Smaller optical bandgaps of about 2 eV have been reported for cobalt oxide [21,22]. The bandgap of 2.0 eV is frequently attributed to single-phase Co_3O_4 while mixed CoO/Co_3O_4 phases have larger bandgaps [23]. In general, cobalt oxide shows more than one optical bandgap, which may depend on the exact composition and on the morphology [23–26].

In the present paper, we utilize a pulsed hollow-cathode (PHC) discharge with a cobalt nickel cathode to deposit mixed cobalt nickel oxide films. The potential of PHC discharges for deposition of thin films has not been fully explored yet. In particular, rather

few investigations regarding the deposition of multi-component films have been reported yet. In this context, PHC discharges using multi-component cathodes are particularly useful. Here, we employ mixed CoNi cathodes with different stoichiometric compositions, e.g., Co20Ni80, Co50Ni50, and Co80Ni20. Films are deposited on Si(111) wafers and on soda lime glass coated with fluorine-doped tin oxide (FTO). The structural, morphological, and optical properties of the deposited films are studied with the help of scanning electron microscopy, X-ray diffraction, Raman spectroscopy, and ellipsometry.

2. Experiment

The experimental set-up has been described elsewhere [27,28]. It consists of a cylindrical hollow cathode (HC) inside a vacuum chamber. The HC is made from cobalt nickel alloy with a purity of 99.95% [28–31]. Several cathodes with different compositions have been employed for film deposition, e.g., Co20Ni80, Co50Ni50, and Co80Ni20, where the numbers indicate the atomic percentage of the cathode material. We use argon and oxygen as working gases at gas flow rates of 200 sccm and 100 sccm, repsectively.

The pulsed hollow cathode is operated with a discharge current of 0.25 A at a repetition frequency of 5 kHz and a pulse length of 100 µs.

Films are deposited on Si(111) or FTO substrates at two different gas pressures (2.8 Pa and 50 Pa) in the vacuum chamber. More details may be found elsewhere [27]. Typical deposition times are 90–120 min.

As-deposited and annealed films are characterized by X-ray diffraction, Raman spectroscopy, and ellipsometry. Annealing is carried out in ambient air using temperatures of 410 °C and 600 °C.

Energy dispersive X-ray spectroscopy (EDX) is employed for the elemental composition analysis of the deposited thin films. The TESCAN Ferra 3 scanning electron microscope (SEM) equipped with an EDAX Octane super 60 mm^2 is employed. Chemical composition analysis is performed with an energy of 15 kV at a working distance of 9 mm. Thickness measurements are performed with an energy of 5 kV at the same distance.

The crystallographic structure of the samples is investigated with the help of the X-ray diffraction (XRD) technique. The Grazing Incidence (GIXRD) geometry with Cu Kα radiation (λ = 0.154 nm) is employed [32]. Raman spectroscopy is carried out at room temperature using a Renishaw Raman Microscope RM 1000.

The optical transmission is measured with a UV-VIS spectrophotometer (LAMBDA 1050 UV/Vis/NIR, Perkin-Elmer). Spectroscopic ellipsometry is conducted at room temperature (300 K) in a dry nitrogen atmosphere with a variable angle ellipsometer (J.A. Woollam VUV-VASE) in the photon energy range 0.8–7.5 eV at three angles of incidence (60°, 65°, and 70°). Refraction index n, extinction coefficient k, and absorption coefficient α are obtained with the help of commercial WVASE software.

The photoelectrochemical (PEC) activity is investigated in an electrochemical cell in a three-electrode configuration. Details may be found elesewhere [27].

3. Results and Discussion

3.1. Film Composition

Deposited films have been analyzed with the help of scanning electron microscopy (SEM). The film thickness is obtained from the cross sectional view of the sample which is cut at the center. The extracted film thickness is 1.98 µm, 3.68 µm, and 1.56 µm for the films deposited with Co20Ni80, Co50Ni50, and Co80Ni20 cathodes, respectively. The film composition of annealed films is measured at two positions (center and near the edge) by EDX. The two results agree well with each other and only the average results are shown in Table 1. The measured film composition and, in particular, the extracted Co/(Co+Ni) ratios agree reasonably with the nominal composition of the considered cathodes.

Table 1. Composition of annealed (600 °C) films on Si(111) substrates for different cathode materials. Gas pressure 50 Pa.

Cathode	Co (at %)	Ni (at %)	O (at %)	Co/(Co+Ni) Ratio
Co20Ni80	14.1	30.7	55.1	0.32
Co50Ni50	24.7	26.9	48.4	0.48
Co80Ni20	54.1	11.9	35.5	0.82

3.2. Crystal Structure

3.2.1. Co50Ni50 Cathode

Figure 1 shows GIXRD results for as-deposited and annealed (at 410 °C and 600 °C) films on Si(111) substrates deposited with the Co50Ni50 cathode at gas pressures of 2.8 Pa and 50 Pa. These films, hence, should contain an approximately equal amount of Co and Ni. The X-ray diffractograms of the as-deposited films show strongly broadened reflections. For the as-deposited films, it was not possible to properly distinguish between pure nickel oxide, cobalt oxide, and/or cobalt nickel oxide phases. The annealed films (410 °C) contain a single crystalline phase which is assigned to cubic nickel oxide (c-NiO) with space group (SG) 225 (ICSD CIF 9866 [33]). We mention in passing that this does not rule out the existence of a mixed $Ni_{1-x}Co_xO$ phase with a c-NiO structure [34] or of an amorphous cobalt-rich phase. In fact, mixed $Ni_{1-x}Co_xO$ phases with a c-NiO lattice structure and x as large as 0.4 (40 at%) have been reported before [34].

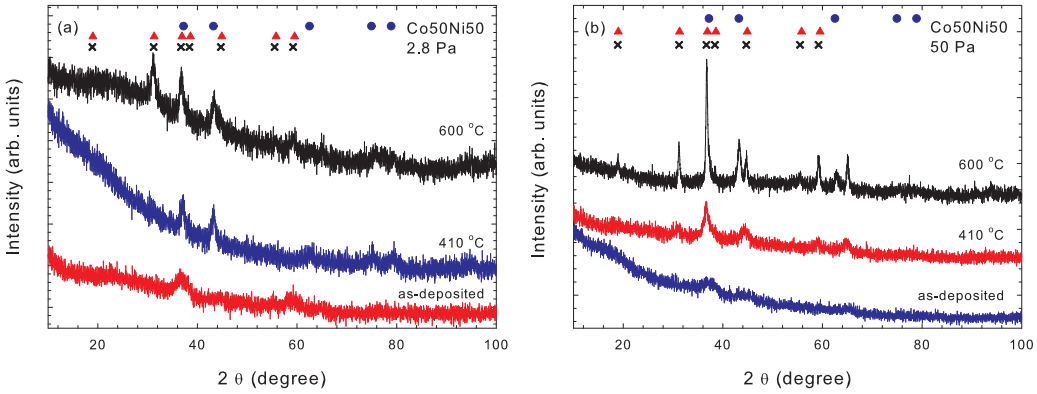

Figure 1. GIXRD of as-deposited and annealed (410 °C, 600 °C) CoNiO films deposited with a Co50Ni50 cathode at (**a**) 2.8 Pa and (**b**) 50 Pa. Reflections from c-NiO (●), c-Co_3O_4 (▲), and c-$NiCo_2O_4$ (×) are indicated.

Annealing at 600 °C results in a phase separation into c-NiO (SG 225) and spinel-type c-Co_3O_4 (SG 227, ICSD CIF 28158 [33]) crystalline phases and leads to an increase in the mean grain size D. Here, *grain* reflects the structural homogenous part in the direction of the diffraction vector and its size is given as a length unit (nm). The mean grain size was evaluated using the Rietveld refinement method (TOPAS software, Bruker). A separation of crystalline phases during annealing has been observed before for CuNiO films [27]. The crystalline phase fractions f of 50% each reflect well the initial composition of the employed Co50Ni50 cathode. No evidence of crystalline CoO or mixed $NiCo_2O_4$ phases was found. Table 2 summarizes the results of our analyses.

3.2.2. Co20Ni80 Cathode

Figure 2 shows the GIXRD results for the nickel-rich films deposited with the Co20Ni80 cathode. Diffractograms of the as-deposited film and of the film annealed at 410 °C show reflections from c-NiO but not from cobalt oxide. Hence, there is no indication of a second crystalline phase. The film deposited at 2.8 Pa has an almost perfect NiO(200) preferred orientation whereas the film deposited at 50 Pa does not show this preference. The reference

value for the lattice parameter of pure c-NiO is 0.4178 nm [33]. The slightly smaller lattice parameters (Table 2) can be explained by a partial incorporation of Co^{2+} (and, eventually, Co^{3+}) ions into the Ni^{2+} lattice sites and the smaller ion radii of Co ions compared to Ni ions [35].

Table 2. Identified crystalline phases and lattice parameters of as-deposited and annealed (410 °C, 600 °C) films deposited at 2.8 Pa and 50 Pa. c = cubic, *f* = crystal phase fraction, *D* = mean grain (particle) size. † = preferred c-NiO(200) orientation, ‡ = cubic phase modification (space group 216), n/e = not evaluable, S/N = poor signal-to-noise ratio.

Film	Crystalline Phase	Lattice Parameter (nm)	*f* (%)	*D* (nm)
		(a1) Co50Ni50—2.8 Pa		
as-deposited	c-Co_3O_4/c-NiO	n/e	n/e	S/N
410 °C	c-NiO	0.4191	100	12
600 °C	c-NiO	0.418	50	13
	c-Co_3O_4	0.810	50	13
		(a2) Co50Ni50—50 Pa		
as-deposited	c-Co_3O_4/c-NiO	n/e	n/e	S/N
410 °C	c-$NiCo_2O_4$	0.8165	100	9
600 °C	c-NiO	0.4176	50	320
	c-Co_3O_4	0.8099	50	200
		(b1) Co20Ni80—2.8 Pa		
as-deposited	c-NiO †	0.4185	100	12
410 °C	c-NiO †	0.4170	100	11
600 °C	c-NiO †	0.4172	87	26
	c-Co_3O_4	0.8104	13	15
		(b2) Co20Ni80—50 Pa		
as-deposited	c-NiO	0.415	100	14
410 °C	c-NiO	0.415	100	17
600 °C	c-NiO	0.4182	83	34
	c-Co_3O_4	0.8078	17	15
		(c1) Co80Ni20—2.8 Pa		
as-deposited	c-Co_3O_4 ‡	0.8139	100	22
410 °C	c-Co_3O_4 ‡	0.8098	100	56
		(c2) Co80Ni20—50 Pa		
as-deposited	c-Co_3O_4/c-NiO	n/e	n/e	S/N
410 °C	c-Co_3O_4‡	0.8078	100	25
600 °C	c-NiO	0.4205	25	200
	c-Co_3O_4	0.8098	75	200

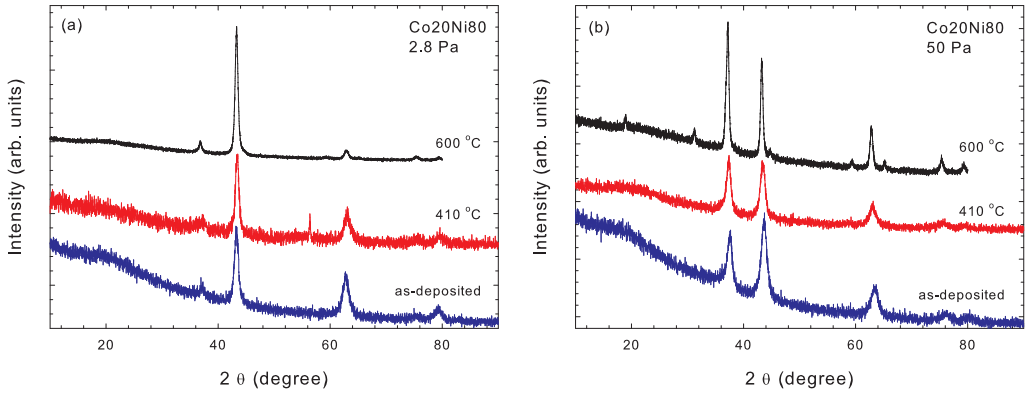

Figure 2. GIXRD of as-deposited and annealed (410 °C, 600 °C) CoNiO films deposited with a Co20Ni80 cathode at (**a**) 2.8 Pa and (**b**) 50 Pa.

Typical crystallite (grain) sizes of the as-deposited and annealed (410 °C) samples are in the range of 11–17 nm. Both diffraction patterns from the as-deposited and annealed (410 °C) sample deposited at 2.8 Pa differ from the 50 Pa sample only in the peak intensities. Annealing at 600 °C leads to a complete separation into cobalt oxide and nickel oxide phases. The results of a quantitative phase analysis with the Rietveld method correspond well with the composition of the employed cathode.

3.2.3. Co80Ni20 Cathode

Figure 3a shows the GIXRD results for the cobalt-rich film deposited at 2.8 Pa with the Co80Ni20 cathode. The diffractograms of the as-deposited film and of the film annealed at 410 °C show the typical reflections from a c-Co_3O_4 phase modification with space group 216 (ICSD CIF 9362). There is no indication of a second crystalline phase. The X-ray diffractogram of the as-deposited film deposited at 50 Pa shows a single reflection in the angular range 36.8–38.1°, which can be attributed to c-NiO, c-Co_3O_4, and/or c-$NiCo_2O_4$ (Figure 3b). It was not possible to distinguish between these crystalline phases due to the strongly broadened line profile, however. Upon annealing at 410 °C, the crystalline phase changes to c-Co_3O_4 (SG 216, ICSD CIF 9362). Mixed $Co_{3-x}Ni_xO_4$ phases with a c-CO_3O_4 lattice structure and x as large as 0.8 (80 at %) have been reported before [34]. Further annealing at 600 °C again leads to a phase separation into c-NiO (SG 225) and c-Co_3O_4 (SG 227, ICSD CIF 28158) and gives rise to large grain sizes of about 200 nm. The extracted Ni/Co ratio of 25/75 is in reasonable agreement to the measured composition (Table 1) and close to the one expected for a Co80Ni20 cathode.

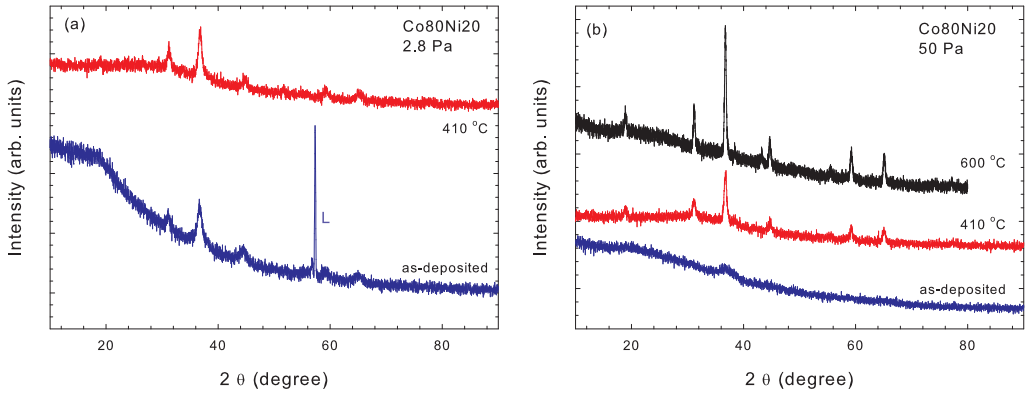

Figure 3. GIXRD of as-deposited and annealed (410 °C, 600 °C) CoNiO films deposited with a Co80Ni20 cathode at (**a**) 2.8 Pa and (**b**) 50 Pa. L = Laue peak.

3.3. Raman Spectroscopy

The GIXRD results are supported by Raman spectroscopy. The as-deposited film from the nickel-rich Co20Ni80 cathode shows a pronounced broad peak at about 545 cm^{-1} and a smaller peak at 1080 cm^{-1} (Figure 4). The peaks are frequently assigned to one-phonon longitudinal optical (LO) mode and two-phonon vibrational modes associated with NiO [15,36,37]. In particular, the one-phonon LO mode at 545 cm^{-1} mode is strongly suppressed in bulk NiO, while it is enhanced in nano-crystalline NiO [38,39]. Similar structures were observed for copper nickel oxide (Cu50Ni50) films [27]. The center wave number of the 545 cm^{-1} peak broadens and shifts to 565 cm^{-1} if the Co50Ni50 cathode is employed. The appearance of two weak shoulders at 480 cm^{-1} and 660 cm^{-1} is indicated. The film deposited with the cobalt-rich Co80Ni20 cathode in addition displays several narrow peaks at 196 cm^{-1}, 480 cm^{-1}, and 680 cm^{-1} which are attributed to Co_3O_4 [27].

The Raman spectra of the annealed films display several narrow peaks at 193 cm^{-1}, 480 cm^{-1}, 525 cm^{-1}, and 680 cm^{-1}, which are attributed to Co_3O_4 (Figure 4) [40,41]. The Raman spectrum obtained with the nickel-rich Co20Ni80 cathode additionally shows a pronounced shoulder at 560 cm^{-1} and a weak peak at 1080 cm^{-1} indicating the presence of

NiO [15,36,37]. The pronounced peak at 680 cm^{-1} is frequently assigned to the A_{1g} mode of Co_3O_4 [29]. The weak band at 193 cm^{-1} is assigned to tetrahedral sites of Co_3O_4 [15].

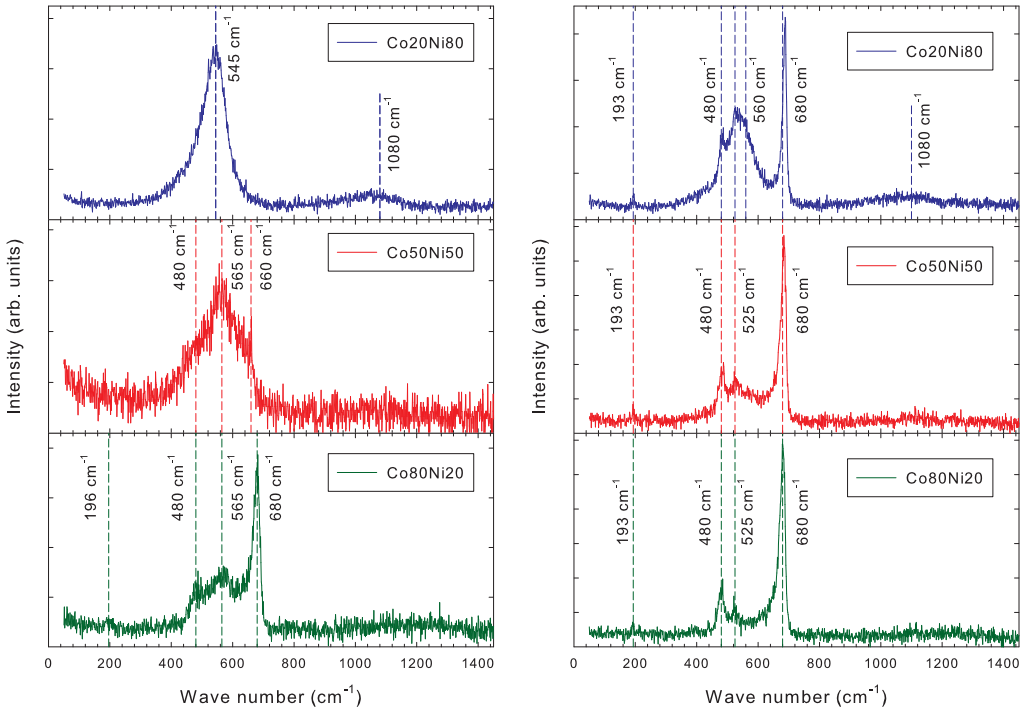

Figure 4. Raman spectroscopy of as-deposited (**left**) and annealed (**right**) films deposited on Si(111) substrates. PHC discharge with three different (Co20Ni80, Co50Ni50, and Co80Ni20) cathodes. Gas pressure 50 Pa.

3.4. Optical Properties

The optical properties of annealed films are investigated by UV-VIS measurements and by ellipsometry. The transmittance of annealed cobalt nickel oxide films deposited on FTO-coated glass using different cathodes obtained from the UV-VIS measurements is displayed in Figure 5a. No corrections regarding the different film thicknesses have been applied. It is evident that films are opaque at small wavelengths below 400 nm and become increasingly transparent at larger wavelengths. This result is further confirmed by our ellipsometry measurements; see below. The transmittance of non-stoichiometric $Co_xNi_{1-x}O$ films was investigated by Roffi et al. [42]. Accordingly, the measured transmittance decreases with increasing cobalt content x, while the absorption edge moves to longer wavelengths (smaller photon energies). These observations are in fair agreement with our results (Figure 5).

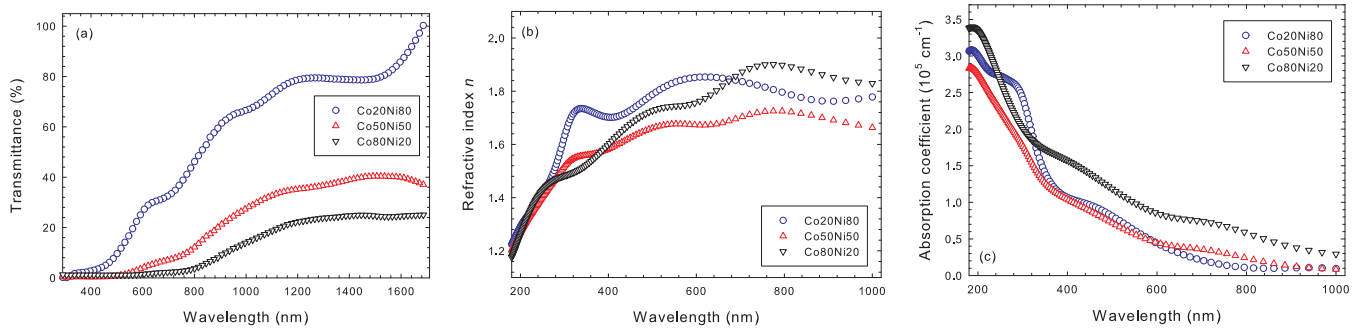

Figure 5. (**a**) Transmittance, (**b**) refractive index n, and (**c**) absorption coefficient α of annealed films (600 °C) on FTO glass obtained with different cathodes: ○ Co20Ni80, △ Co50Ni50, and ▽ Co80Ni20.

The optical properties of films deposited at 50 Pa on FTO-coated glass and annealed at 600 °C are further obtained from ellipsometry measurements. Figure 5b displays the refractive index n, which increases (decreases) with wavelength λ (photon energy E_{ph}) from about $n \approx 1.2$ at $\lambda = 180$ nm ($E_{ph} = 6.9$ eV) to $n \approx 1.8$ at $\lambda = 1000$ nm ($E_{ph} = 1.24$ eV). Only minor differences are observed for the three samples deposited with different cathode compositions (Co20Ni80, Co50Ni50, and Co80Ni80). The absorption coefficient for these films is displayed in Figure 5c as function of wavelength. Again, the present ellipsometry results show that all films become opaque at small wavelengths and increasingly transparent at larger wavelengths. A similar behavior of the absorbance was observed before [43]. The absorption behavior is rather complicated, however, showing more than one absorption edge corresponding to several optical bandgaps [44–46].

A more thorough analysis of the absorption behavior employing a so-called Tauc plot making use of

$$(\alpha\, E_{ph})^2 = E_{ph} - E_g \quad (1)$$

is shown in Figure 6, where α is the absorption coefficient and E_{ph} is the photon energy [47]. A direct optical bandgap as in the case of CoO, Co_3O_4, and NiO is assumed [48–50]. From this plot we derive optical bandgaps of 4.14 eV, 4.20 eV, and 4.14 eV for copper nickel oxide films obtained with the Co20Ni80, Co50Ni50, and Co80Ni20 cathodes, respectively. There is an indication of a second optical bandgap at 3.50 eV for the Co20Ni80 cathode. NiO has a direct optical bandgap of about 3.8 eV [18–20,51–53]. A similar optical bandgap is observed for CoO [53]. Slightly larger bandgap energies of 3.88 eV/4.07 eV [54] and 4.38 eV [8] are reported for $NiCo_2O_4$. However, our XRD data for the annealed films reveal no evidence of crystalline CoO or $NiCo_2O_4$ phases. The bandgap of ≈4.15 eV observed here is, hence, assigned to the nickel oxide composition of the annealed films.

Smaller optical bandgaps are reported for cobalt oxide [21,22]. In general, cobalt oxide shows several optical bandgaps which depend on the composition and on the morphology. An expanded view of the photon energy region below 3.5 eV is displayed in the inset of Figure 6. Direct optical bandgaps of 2.10 eV, 2.23 eV, and 2.19 eV for the Co20Ni80, Co50Ni50, and Co80Ni20 cathodes, respectively, are extracted from this graph. The extracted bandgaps agree well with the reported optical bandgap of about 2.17 eV for Co_3O_4 [23–26,55]. The result is further supported by our XRD analysis.

Finally, we mention in passing that films deposited on FTO-coated glass are also tested for photoelectrochemical activity using the same set-up as for CuNiO films [27]. Na_2SO_4 and NaOH are employed as electrolytes. No photoelectrochemical activity of the present copper nickel oxide has been observed, however.

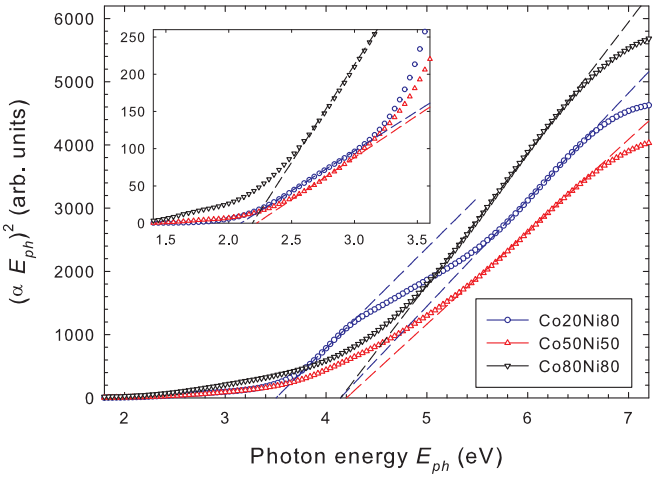

Figure 6. Tauc plot assuming a direct bandgap for annealed films (600 °C) deposited on FTO glass with different cathodes: ○ Co20Ni80, △ Co50Ni50, and ▽ Co80Ni20. Inset shows expanded view between 1.5 eV and 3.5 eV.

4. Conclusions

Results are reported for mixed cobalt nickel oxide films deposited with the help of a pulsed hollow-cathode (PHC) discharge operated at 5 kHz. Deposited films are composed of a mixed metal oxide (MMO) phase. During annealing at 600 °C, the MMO phase separates into two crystalline cubic Co_3O_4 and cubic NiO subphases. The results are confirmed by Raman spectroscopy. The refraction index and absorption coefficient are derived from ellipsometry measurements. The refractive index increases from 1.2 at 200 nm to about 1.8 at 1000 nm. Annealed films are opaque at small wavelengths and become increasingly more transparent at longer wavelengths. Optical bandgaps of about 4.15 eV are linked to the NiO phase of the annealed films, while a second optical bandgap at about 2.17 eV is linked to the Co_3O_4 phase. Photoelectrochemical activity was not observed.

Author Contributions: Conceptualization, R.H., M.C. and Z.H.; Methodology, R.H. and L.V.; Formal analysis, N.N.; Investigation, A.K., R.H., J.O., A.P. and N.N.; Resources, M.C. and Z.H.; Data curation, A.K., R.H. and H.W.; Writing—original draft, R.H.; Writing—review & editing, H.W., M.C. and Z.H. All authors have read and agreed to the published version of the manuscript.

Funding: This research was funded by Technology Agency of the Czech Republic grant number FW06010462.

Institutional Review Board Statement: Not applicable.

Informed Consent Statement: Not applicable.

Data Availability Statement: Data are contained within the article.

Conflicts of Interest: The authors declare no conflicts of interest.

References

1. Poonam; Sharma, K.; Singh, N.; Tripathi, S.K. Characterization of nickel cobalt oxide: A potential material for supercapacitor. *Mater. Res. Express* **2018**, *6*, 025502. [CrossRef]
2. Huang, X.; Wu, J.; Guo, R.; Lin, Y.; Zhang, P. Aligned nickel–cobalt oxide nanosheet arrays for lithium ion battery applications. *Int. J. Hydrogen Energy* **2014**, *39*, 21399–21404. [CrossRef]
3. Masoud, E.M. Improved initial discharge capacity of nanostructured Ni-Co spinel ferrite as anode material in lithium ion batteries. *Solid State Ionics* **2013**, *253*, 247–252. [CrossRef]
4. He, Q.; Gu, S.; Wu, T.; Zhang, S.; Ao, X.; Yang, J.; Wen, Z. Self-supported mesoporous $FeCo_2O_4$ nanosheets as high capacity anode material for sodium-ion battery. *Chem. Eng. J.* **2017**, *330*, 764–773. [CrossRef]
5. Sharma, Y.; Sharma, N.; Subbarao, G.; Chowdari, B. Studies on spinel cobaltites, $FeCo_2O_4$ and $MgCo_2O_4$ as anodes for Li-ion batteries. *Solid State Ionics* **2008**, *179*, 587–597. [CrossRef]
6. Julien, C.; Gendron, F.; Amdouni, A.; Massot, M. Lattice vibrations of materials for lithium rechargeable batteries. VI: Ordered spinels. *Mater. Sci. Eng. B* **2006**, *130*, 41–48. [CrossRef]
7. Chavhan, M.P.; Sethi, S.R.; Ganguly, S. Mixed metal oxides in synergy at nanoscale: Electrospray induced porosity of in situ grown film electrode for use in electrochemical capacitor. *Electrochim. Acta* **2020**, *347*, 136277. [CrossRef]
8. Pradeepa, S.S.; Rajkumar, P.; Diwakar, K.; Sutharthani, K.; Subadevi, R.; Sivakumar, M. A Facile One-Pot Hydrothermal Synthesis of Zn, Mn Co-Doped NiCo2O4 as an Efficient Electrode for Supercapacitor Applications. *ChemistrySelect* **2021**, *6*, 6851–6862. [CrossRef]
9. Hong, W.-L.; Lin, L.-Y. Design of nickel cobalt oxide and nickel cobalt oxide@nickel molybdenum oxide battery-type materials for flexible solid-state battery supercapacitor hybrids. *J. Power Sources* **2019**, *435*, 226797. [CrossRef]
10. Banno, S.; Imanaka, N.; Adachi, G. Selective nitrogen dioxide sensor based on nickel copper oxide mixed with rare earths. *Sens. Actuators B Chem.* **1995**, *25*, 619–622. [CrossRef]
11. Lee, J.H.; Noh, Y.W.; Jin, I.S.; Park, S.H.; Jung, J.W. Efficient perovskite solar cells with negligible hysteresis achieved by sol–gel-driven spinel nickel cobalt oxide thin films as the hole transport layer. *J. Mater. Chem. C* **2019**, *7*, 7288–7298. [CrossRef]
12. Vidales, A.G.; Choi, K.; Omanovic, S. Nickel-cobalt-oxide cathodes for hydrogen production by water electrolysis in acidic and alkaline media. *Int. J. Hydrogen Energy* **2018**, *43*, 12917–12928. [CrossRef]
13. Yentekakis, I.V.; Panagiotopoulou, P.; Artemakis, G. A review of recent efforts to promote dry reforming of methane (DRM) to syngas production via bimetallic catalyst formulations. *Appl. Catal. B Environ.* **2021**, *296*, 120210. [CrossRef]
14. Kongsawatvoragul, K.; Kalasina, S.; Phattharasupakun, N.; Sawangphruk, M. A single energy conversion and storage cell of nickel-doped cobalt oxide under UV and visible light illumination. *Electrochim. Acta* **2019**, *328*, 135120. [CrossRef]

15. Jirátová, K.; Čada, M.; Naiko, I.; Ostapenko, A.; Balabánová, J.; Koštejn, M.; Maixner, J.; Babii, T.; Topka, P.; Soukup, K.; et al. Plasma Jet Sputtering as an Efficient Method for the Deposition of Nickel and Cobalt Mixed Oxides on Stainless-Steel Meshes: Application to VOC Oxidation. *Catalysts* **2022**, *13*, 79. [CrossRef]
16. Jirátová, K.; Soukal, P.; Kapran, A.; Babii, T.; Balabánová, J.; Koštejn, M.; Čada, M.; Maixner, J.; Topka, P.; Hubička, Z.; et al. Nickel-Copper Oxide Catalysts Deposited on Stainless Steel Meshes by Plasma Jet Sputtering: Comparison with Granular Analogues and Synergistic Effect in VOC Oxidation. *Catalysts* **2023**, *13*, 595. [CrossRef]
17. Peng, T.; Xiao, X.; Han, X.; Zhou, X.; Wu, W.; Ren, F.; Jiang, C. Characterization of DC reactive magnetron sputtered NiO films using spectroscopic ellipsometry. *Appl. Surf. Sci.* **2011**, *257*, 5908–5912. [CrossRef]
18. Duraisamy, N.; Kandiah, K.; Rajendran, R.; S, P.; R, R.; Dhanaraj, G. Electrochemical and photocatalytic investigation of nickel oxide for energy storage and wastewater treatment. *Res. Chem. Intermed.* **2018**, *44*, 5653–5667. [CrossRef]
19. Awais, M.; Rahman, M.; MacElroy, J.D.; Coburn, N.; Dini, D.; Vos, J.G.; Dowling, D.P. Deposition and characterization of NiOx coatings by magnetron sputtering for application in dye-sensitized solar cells. *Surf. Coat. Technol.* **2010**, *204*, 2729–2736. [CrossRef]
20. Sato, H.; Minami, T.; Takata, S.; Yamada, T. Transparent conducting p-type NiO thin films prepared by magnetron sputtering. *Thin Solid Films* **1993**, *236*, 27–31. [CrossRef]
21. Hong, T.; Liu, Z.; Zheng, X.; Zhang, J.; Yan, L. Efficient photoelectrochemical water splitting over Co_3O_4 and Co_3O_4/Ag composite structure. *Appl. Catal. B Environ.* **2017**, *202*, 454–459. [CrossRef]
22. Moridon, S.N.F.; Salehmin, M.N.I.; Arifin, K.; Minggu, L.J.; Kassim, M.B. Synthesis of Cobalt Oxide on FTO by Hydrothermal Method for Photoelectrochemical Water Splitting Application. *Appl. Sci.* **2021**, *11*, 3031. [CrossRef]
23. Jung, S.; Nandi, D.K.; Yeo, S.; Kim, H.; Jang, Y.; Bae, J.-S.; Hong, T.E.; Kim, S.-H. Phase-controlled growth of cobalt oxide thin films by atomic layer deposition. *Surf. Coat. Technol.* **2018**, *337*, 404–410. [CrossRef]
24. Al-Tuwirqi, R.M.; Al-Hazmi, F.; Alnowaiser, F.; Al-Ghamdi, A.A.; Aal, N.A.; El-Tantawy, F. Synthesis and physical properties of mixed Co3O4/CoO nanorods by microwave hydrothermal technique. *Superlattices Microstruct.* **2011**, *50*, 437–448. [CrossRef]
25. Barakat, N.A.M.; Khil, M.S.; Sheikh, F.A.; Kim, H.Y. Synthesis and Optical Properties of Two Cobalt Oxides (CoO and Co3O4) Nanofibers Produced by Electrospinning Process. *J. Phys. Chem. C* **2008**, *112*, 12225–12233. [CrossRef]
26. Prieto, P.; Marco, J.; Serrano, A.; Manso, M.; de la Figuera, J. Highly oriented (111) CoO and Co_3O_4 thin films grown by ion beam sputtering. *J. Alloys Compd.* **2019**, *810*, 151912. [CrossRef]
27. Kapran, A.; Hippler, R.; Wulff, H.; Olejnicek, J.; Pisarikova, A.; Cada, M.; Hubicka, Z. Characteristics of a pulsed hollow cathode discharge operated in an Ar+O2 gas mixture and deposition of copper nickel oxide thin films. *Vacuum* **2023**, *215*, 112272. [CrossRef]
28. Hippler, R.; Cada, M.; Hubicka, Z. A positively biased external anode for energy control of plasma ions: Hollow cathode and magnetron sputtering discharge. *Plasma Sources Sci. Technol.* **2021**, *30*, 045003. [CrossRef]
29. Olejníček, J.; Šmíd, J.; Perekrestov, R.; Ksirova, P.; Rathouský, J.; Kohout, M.; Dvořáková, M.; Kment, Š.; Jurek, K.; Čada, M.; et al. Co3O4 thin films prepared by hollow cathode discharge. *Surf. Coat. Technol.* **2019**, *366*, 303–310. [CrossRef]
30. Olejníček, J.; Šmíd, J.; Čada, M.; Kšírová, P.; Kohout, M.; Perekrestov, R.; Tvarog, D.; Kment, Š.; Kmentová, H.; Hubička, Z. High rate deposition of photoactive TiO2 films by hot hollow cathode. *Surf. Coat. Technol.* **2020**, *383*, 125256. [CrossRef]
31. Olejníček, J.; Hrubantová, A.; Volfová, L.; Dvořáková, M.; Kohout, M.; Tvarog, D.; Gedeon, O.; Wulff, H.; Hippler, R.; Hubička, Z. WO_3 and WO_{3-x} thin films prepared by DC hollow cathode discharge. *Vacuum* **2021**, *195*, 110679. [CrossRef]
32. Wulff, H.; Steffen, H. Characterization of Thin Films. In *Low Temperature Plasmas*; Hippler, R., Kersten, H., Schmidt, M., Schoenbach, K.-H., Eds.; Wiley-VCH: Berlin, Germany, 2008; pp. 329–362.
33. ICSD, Inorganic Crystal Structure Database, FIZ Karlsruhe—Leibniz-Institut für Informationsinfrastruktur GmbH. Eggenstein-Leopoldshafen, Germany. Available online: https://icsd.products.fiz-karlsruhe.de/ (accessed on 25 February 2024).
34. De Faria, L.; Prestat, M.; Koenig, J.-F.; Chartier, P.; Trasatti, S. Surface properties of Ni+Co mixed oxides: A study by X-rays, XPS, BET and PZC. *Electrochim. Acta* **1998**, *44*, 1481–1489. [CrossRef]
35. Shannon, R.D. Revised effective ionic radii and systematic studies of interatomic distances in halides and chalcogenides. *Acta Cryst.* **1976**, *A32*, 751–766. [CrossRef]
36. Javadian, A.; Fadavieslam, M.R. Impact of copper doping in NiO thin films deposited by spray pyrolysis on their physical properties. *J. Mater. Sci. Mater. Electron.* **2022**, *33*, 23362–23374. [CrossRef]
37. Mahala, C.; Basu, M. Nanosheets of NiCo2O4/NiO as Efficient and Stable Electrocatalyst for Oxygen Evolution Reaction. *ACS Omega* **2017**, *2*, 7559–7567. [CrossRef]
38. Duan, W.J.; Lu, S.H.; Wu, Z.L.; Wang, Y.S. Size Effects on Properties of NiO Nanoparticles Grown in Alkalisalts. *J. Phys. Chem. C* **2012**, *116*, 26043–26051. [CrossRef]
39. Mironova-Ulmane, N.; Kuzmin, A.; Sildos, I.; Puust, L.; Grabis, J. Magnon and Phonon Excitations in Nanosized NiO. *Latv. J. Phys. Tech. Sci.* **2019**, *56*, 61–72. [CrossRef]
40. Hippler, R.; Cada, M.; Ksirova, P.; Olejnicek, J.; Jiricek, P.; Houdkova, J.; Wulff, H.; Kruth, A.; Helm, C.; Hubicka, Z. Deposition of cobalt oxide films by reactive pulsed magnetron sputtering. *Surf. Coat. Technol.* **2021**, *405*, 126590. [CrossRef]
41. Hadjiev, V.G.; Iliev, M.; Vergilov, I.V. The Raman spectra of Co_3O_4. *J. Phys. C Solid State Phys.* **1988**, *21*, L199–L201. [CrossRef]
42. Roffi, T.M.; Uchida, K.; Nozaki, S. Structural, electrical, and optical properties of $Co_xNi_{1-x}O$ films grown by metalorganic chemical vapor deposition. *J. Cryst. Growth* **2015**, *414*, 123–129. [CrossRef]

43. Fernández, C.d.J.; Mattei, G.; Sada, C.; Battaglin, C.; Mazzoldi, P. Nanostructural and optical properties of cobalt and nickel–oxide/silica nanocomposites. *Mater. Sci. Eng. C* **2006**, *26*, 987–991. [CrossRef]
44. Cui, B.; Lin, H.; Liu, Y.-Z.; Li, J.-B.; Sun, P.; Zhao, X.-C.; Liu, C.-J. Photophysical and Photocatalytic Properties of Core-Ring Structured NiCo2O4 Nanoplatelets. *J. Phys. Chem. C* **2009**, *113*, 14083–14087. [CrossRef]
45. Bitla, Y.; Chin, Y.-Y.; Lin, J.-C.; Van, C.N.; Liu, R.; Zhu, Y.; Liu, H.-J.; Zhan, Q.; Lin, H.-J.; Chen, C.-T.; et al. Origin of metallic behavior in NiCo2O4 ferrimagnet. *Sci. Rep.* **2015**, *5*, 15201–15201. [CrossRef] [PubMed]
46. Nashaat, A.M.; Abu El-Fadl, A.; Nakamura, H.; Kassem, M.A. Glassy magnetic freezing and exchange bias effect in NiCo2O4/(Co-Ni)O nanoparticles composite. *J. Magn. Magn. Mater.* **2023**, *567*, 170366. [CrossRef]
47. Tauc, J.; Grigorovici, R.; Vancu, A. Optical Properties and Electronic Structure of Amorphous Germanium. *Phys. Status Solidi B* **1966**, *15*, 627–637. [CrossRef]
48. Mane, A.U.; Shivashankar, S. MOCVD of cobalt oxide thin films: Dependence of growth, microstructure, and optical properties on the source of oxidation. *J. Cryst. Growth* **2003**, *254*, 368–377. [CrossRef]
49. Pandey, V.; Adiba, A.; Munjal, S.; Ahmad, T. Optical bandgap tuning of cubic spinel Co_3O_4 by annealing temperature. *Materialia* **2022**, *26*, 101554. [CrossRef]
50. Manjunatha, K.N.; Paul, S. Investigation of optical properties of nickel oxide thin films deposited on different substrates. *Appl. Surf. Sci.* **2015**, *352*, 10–15. [CrossRef]
51. Rajesh, M.; Vengatesan, K.; Aly, M.H.; Sitharthan, R.; Dhanabalan, S.S.; Karthikeyan, M. Electrical and optical properties of sol–gel-deposited NiO films and corresponding response to annealing temperature. *Opt. Quantum Electron.* **2023**, *55*, 1167. [CrossRef]
52. Lahiji, F.A.F.; Bairagi, S.; Magnusson, R.; Sortica, M.A.; Primetzhofer, D.; Ekström, E.; Paul, B.; le Febvrier, A.; Eklund, P. Growth and optical properties of NiO thin films deposited by pulsed dc reactive magnetron sputtering. *J. Vac. Sci. Technol. A* **2023**, *41*, 063402. [CrossRef]
53. Powell, R.J.; Spicer, W.E. Optical Properties of NiO and CoO. *Phys. Rev. B* **1970**, *2*, 2182–2193. [CrossRef]
54. Silambarasan, M.; Ramesh, P.S.; Geetha, D. Facile one-step synthesis, structural, optical and electrochemical properties of NiCo2O4 nanostructures. *J. Mater. Sci. Mater. Electron.* **2016**, *28*, 323–336. [CrossRef]
55. Louardi, A.; Rmili, A.; Chtouki, T.; Elidrissi, B.; Erguig, H.; El Bachiri, A.; Ammous, K.; Mejbri, H. Effect of annealing treatment on Co_3O_4 thin films properties prepared by spray pyrolysis. *J. Mater. Environ. Sci.* **2017**, *8*, 485.